RSC Advances

PAPER

View Article Online
View Journal | View Issue

Cite this: *RSC Adv.*, 2025, **15**, 17241

Mechanistic insights into base-free nickel-catalyzed Suzuki–Miyaura cross-coupling of acid fluoride and the origin of chemoselectivity: a DFT study†

Wasihun Menberu Dagnaw, *[a] Yohannes Mulugeta Hailu [b] and Ahmed M. Mohammed[c]

Palladium-catalyzed Suzuki–Miyaura Coupling (SMC) is a powerful strategy to construct C–C bonds; however, it suffers from the disadvantages of using expensive palladium catalysts and additives. Based on the experimental development of the base-free nickel catalyzed Suzuki–Miyaura coupling of acid fluorides (ArC(O)F) with diboron reagent, we carried out DFT calculations to gain insight into the reaction mechanisms. The coupling reaction proceeds *via* four stages: (1) oxidative addition of the acid fluoride to the Ni(0) center to break the C–F bond, (2) transmetalation with diboron reagent, (3) carbonyl deinsertion *via* reverse carbonyl migratory insertion, and (4) reductive elimination to afford the coupling product and regenerate the active catalyst. It was found that the competitive rotation of the Ni–B bond and Ni–C(aryl) bond of the intermediate generated from the oxidative addition of the acid fluoride to Ni(0) center (stage I) determines the chemoselectivity of the catalytic cycle, and carbonyl migratory insertion is the rate-determining step of the coupling. Our study reveals that the PhOMe moiety in **TS8** induces greater steric hindrance and reduced electronic stabilization compared to BPin in **TS5**, resulting in increased geometric distortion, higher distortion energy, and a less favorable transition state with a higher activation barrier. Furthermore, our computational results indicate that transmetalation prefers a concerted mechanism. Detailed analyses reveals that the strong fluorophilicity of boron enables efficient, base-free transmetalation. This study could be helpful for the development of cheap catalysts for Suzuki–Miyaura cross-coupling reactions.

Received 15th March 2025
Accepted 5th May 2025

DOI: 10.1039/d5ra01845e

rsc.li/rsc-advances

1. Introduction

The palladium-catalyzed Suzuki–Miyaura coupling is a powerful strategy to construct C–C bond forming reactions, which consist of the coupling between organoboron nucleophiles and aryl halide (or triflate) electrophiles in the presence of a base,[1–5] often used in organic, medicinal and agrichemical industries.[6–9] The key challenges associated with this transformation are the use of expensive palladium catalysts, the addition of exogenous base to facilitate transmetalation and requirement of expensive and rare electrophiles.[10,11] To further address these challenges significant efforts have been devoted to replacing palladium with nickel for the development of different SMC reactions in the presence of an exogenous base.[12–17] Ideally, using cheap and earth–abundant transition metal (*e.g.*, Ni) catalysts with available electrophiles in the absence of an exogenous base is the most preferred way to carry out SMC reactions.[18–21] In 2018, Sanford and coworkers made a breakthrough, discovery that a nickel (Ni) complex could serve as a catalyst for the coupling reaction between aryl boronic acids and acid fluorides, in the absence of an exogenous base (Fig. 1 eqn (a)).[22] Recently, the same group developed a base free nickel-catalyzed

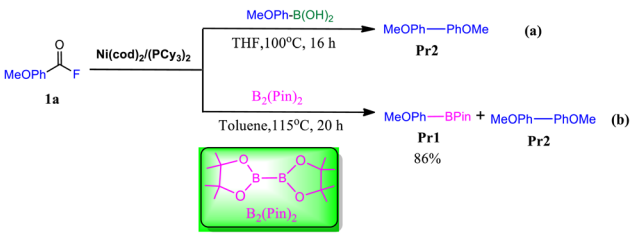

Fig. 1 Base-free nickel catalysed decarbonylative Suzuki–Miyaura-type reactions.[22,23]

[a]*Department of Chemistry, College of Natural Sciences, Haramaya University, Dire Dawa, P.O. Box 138, Ethiopia. E-mail: wasihunmenberu@yahoo.com*

[b]*Department of Chemical Engineering, National Taiwan University of Science and Technology, Taipei, Taiwan, Republic of China*

[c]*Department of Chemistry, College of Natural and Computational Sciences, Addis Ababa University, P.O. Box 1176, Addis Ababa, Ethiopia*

† Electronic supplementary information (ESI) available. See DOI: https://doi.org/10.1039/d5ra01845e

decrbonylative coupling of carboxylic acid fluorides with diboron reagent to selectively afford aryl boronate ester products (Fig. 1 eqn (b)).[23] However, a primary challenge associated with this metal-catalyzed borylation reaction is that the competing of organoboron product *versus* the diboron reagent in the transmetalation step, leading to undesired over cross-coupling to afford biaryl byproduct (Fig. 1 eqn (b)).[23]

Recently, we[24] reported a DFT study of the base-free Ni-catalyzed Suzuki–Miyaura cross-coupling of acid fluoride by Sanford and co-worker,[22] where we found that the transmetalation proceeds through a stepwise mechanism, instead of the conventional concerted one. Additionally, the strong fluorophilicity of boron and the coordination interaction between the oxygen atom of boronic acid with Ni metal plays a vital role in promoting the base free transmetalation. Herein, we theoretically studied the Suzuki–Miyaura cross-coupling mechanism of the base-free nickel-catalyzed decarbonylative borylation of acid fluorides, to reveal the origin of the chemoselectivity to aryl boronate ester over biaryl. Indeed, our calculation showed that the decarbonylation step occurs after transmetalation; which further supports our previous finding.[24] Our understanding of the substrate-dependent chemoselectivity should be helpful for development of cheap catalysts for Suzuki–Miyaura cross-coupling reactions between acid fluoride and diboron reagent.

2. Computational methods

All the DFT calculations were carried out using the Gaussian 09 program.[25] All structures were optimized in the gas phase at B3LYP[26,27]/BSI level, where BSI represents a basis set with 6-31G(d,p)[28–31] for nonmetal atoms and SDD[32,33] for Ni. Harmonic vibrational frequency calculations were subsequently performed to verify the optimized structures to be minimal (no imaginary frequency) or transition states (TSs, having a unique one imaginary frequency). The energies were then improved by M06 (ref. 34–36)/BSII//B3LYP/BSI single-point calculations with solvent effects accounted by SMD[37,38] solvent model, using the experimental solvent, toluene. BSII denotes a basis set with SDD for Ni and 6-311++G(d,p) for other atoms. Additional information is relegated to ESI.† Selected optimized structures are illustrated using CYLview.[39]

3. Results and discussion

Sanford *et al.*[23] have shown their strategy to synthesize aryl boronate ester from acid fluoride and diboron reagent (Fig. 2). At first, the oxidative addition of the acid fluoride substrate to $Ni^0(PCy_3)_2$ to yield an acyl Ni specious (**I**), thus carbonyl deinsertion to afford transmetalation active complex (**II**), then transmetalation with diboron reagent, C–B bond-forming reductive elimination afford the product and regenerate $Ni^0(PCy_3)_2$. Furthermore, the over cross-coupling of aryl boronate ester leads to biaryl formation. In the following, we report our DFT study results to gain insight into the mechanisms of the reactions and disclose the origin of chemoselectivity.

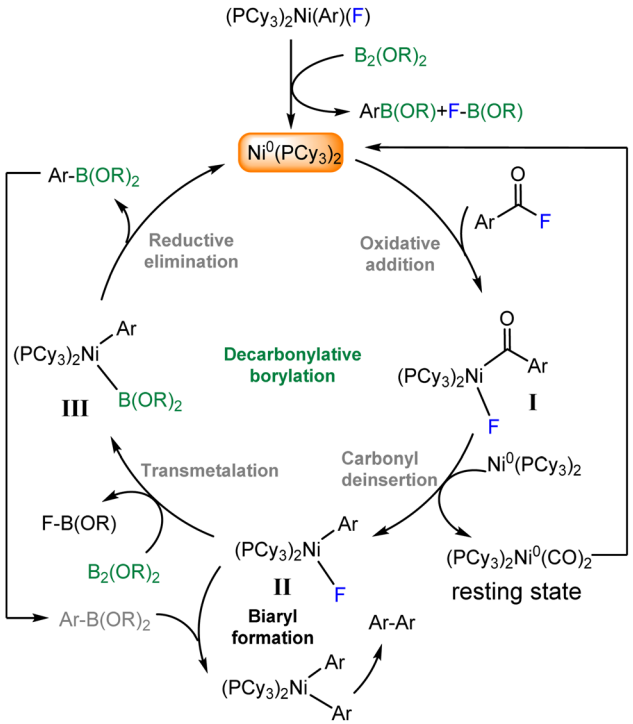

Fig. 2 Experimentally postulated mechanism for organoboron and biaryl synthesis from acid fluoride and diboron reagent by Sanford *et al.*[23]

3.1 The mechanism for base-free Ni-catalyzed decarbonylative borylation

Based on our previous theoretical study on nickel-catalyzed Suzuki–Miyaura coupling of acid fluorides (ArC(O)F) with boronic acids (Ar′B(OH),[24] **Cat** is regarded as the real catalyst which can be generated from the $Ni(Cod)_2$ as the catalyst precursor and two equivalents of PCy_3 ligand,[24] Fig. 3 shows the energy profile for oxidative addition and decarbonylation stages in Fig. 1(b). Similarly, the initial stage of the reaction is an oxidative addition of the acidic fluoride (**1a**) to Ni(0) center *via* **TS1** with a free energy barrier of 17.6 kcal mol^{-1} to reversibly form a tetrahedral geometry **IM1**. Subsequently, **IM1** can be easily transformed to a 17.0 kcal mol^{-1} more stable square planar geometry **IM2**. To undergo decarbonylation, a PCy_3 ligand dissociates from **IM2** *via* **TS2** with a barrier of 23.7 kcal-mol^{-1}, giving **IM3** with a vacant coordination site. Because **IM2** is a saturated complex, a ligand should dissociate from Ni-center to allow decarbonylation. Next, a carbonyl migratory insertion occurs *via* **TS3** with a low barrier of 2.1 kcal mol^{-1} from **IM3** to give a carbonyl nickel fluoride complex **IM4**. Subsequent liberation of CO from **IM4** gives **IM5** which either associates with a released PCy_3 ligand to reach more stable **IM6** or proceeds to the next stage of transmetalation with diboron reagent (B_2Pin_2). However, the possible dissociation intermediate has higher energy barrier of 32.7 kcal mol^{-1} relative to **IM2** and we excluded the possibility without further consideration. The results indicated that direct decarbonylation after oxidative addition is unlikely, encouraging us to find an alternative.

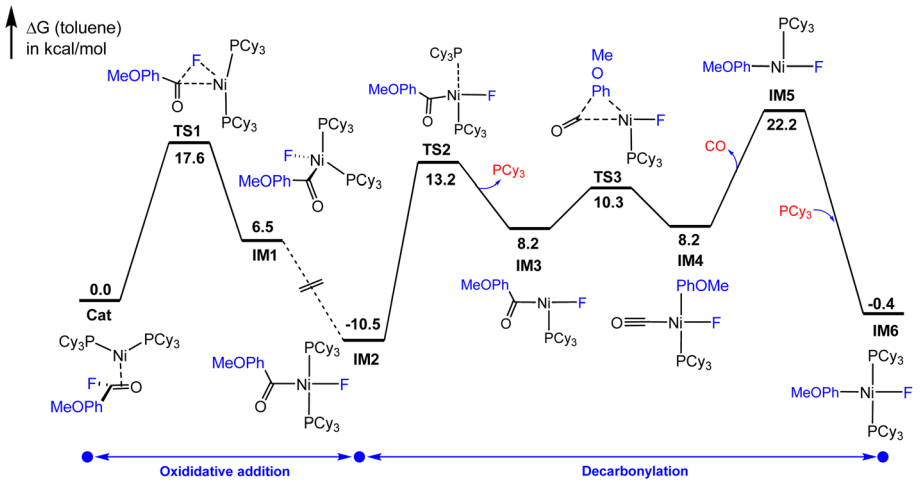

Fig. 3 Free-energy profiles for oxidative addition and decarbonylation stages in Fig. 1(b).

Previously, we also ruled out the direct decarbonylation after oxidative addition.[24]

Alternatively, we also considered the possibility of **IM2** to directly undergo transmetalation. Fig. 4 describes the alternative where the transmetalation takes place first. Note that, in Fig. 3 the decarbonylation occurs after oxidative addition. The optimized structures of selected intermediates and transition state are shown in Fig. 5. Previously, we considered two transmetalation pathways.[24] Starting from **IM2**, the concerted mechanism (black line) occurs *via* **TS4** crosses a barrier of 16.8 kcal mol^{-1} and is slightly endergonic by 1.5 kcal mol^{-1} to form **IM7**. The calculated result agrees with the conventional transmetalation. Previously, we considered a stepwise mechanism.[24] Unfortunately, we were not able to locate the transition state after several attempts made. However, the possible coordinative intermediate **IM8** (ΔG = 8.4 kcal mol^{-1}) is 2.1 kcal mol^{-1} higher than the concerted **TS4** (ΔG = 6.3 kcal mol^{-1}) and can be excluded. Starting from **IM7** the carbonyl migratory insertion requires rotating the Bpin group *trans* to the carbonyl group, as illustrated by **TS5** in Fig. 4 which crosses a barrier of 21.9 kcal mol^{-1} relative to **IM7**. Alternatively, we also considered the possibility of rotating the PCy_3 to undergo a carbonyl migratory insertion. However, as illustrated in ESI (Fig S.2),† we found that the calculated free energy barrier for the possible CO dissociation intermediate **IM11A** is 4.6 kcal mol^{-1} higher than **TS5**, which revealed that the mechanism following rotating the PCy_3 is unfavorable. Then, a carbonyl migratory insertion proceeds *via* **TS6**, generates more

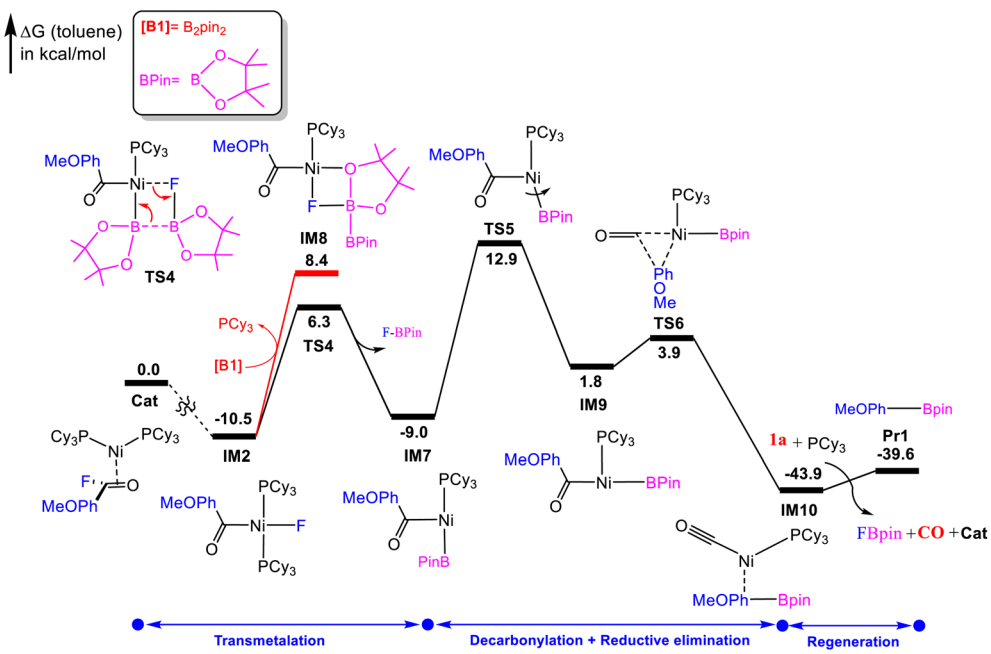

Fig. 4 Free-energy profiles for the mechanism *via* transmetalation, decarbonylation and catalyst regeneration, leading **Pr1**.

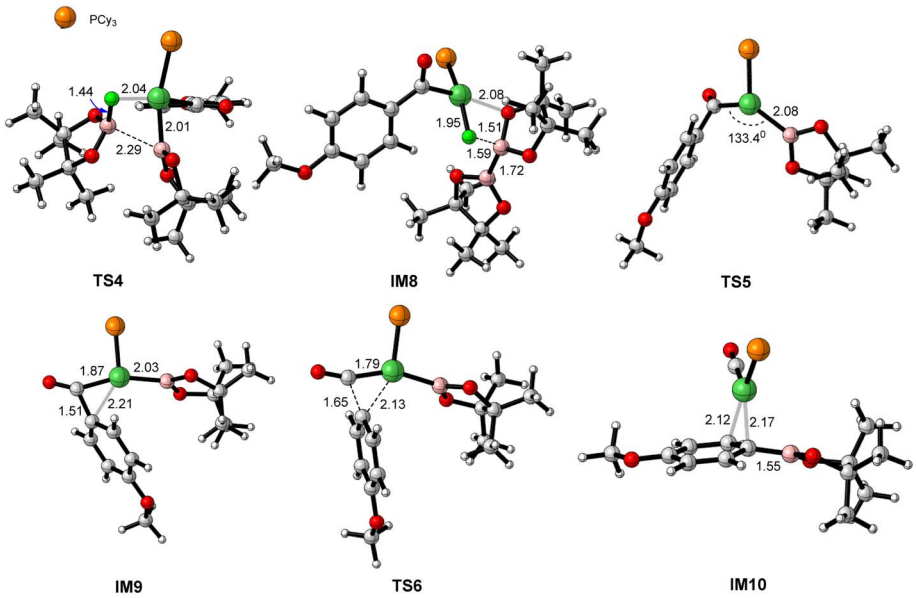

Fig. 5 Optimized structures of the key stationary points labeled in Fig. 4.

stable the CO-coordinated Ar[Ni](CO)Bpin intermediate **IM10**. To confirm both sides of the potential energy surface, we performed the IRC calculation for TS6. The result shows a concerted mechanism involving both carbonyl migratory insertion and reductive elimination takes place simultaneously (as evidenced by the slight elongation of the Ni–CO bond length in the forward IRC pathway, continuing from P3 (1.784 Å) to P4 (1.809 Å) and consequently from P4 (1.809 Å to IM10 (1.813 Å) (see Fig. S.3†). Finally, CO liberation helps to recover the catalyst and the coupling product (**Pr1**). Overall, the carbonyl migratory insertion has a rate-determining step (RDS) with a barrier of 23.4 kcal mol^{-1} (**TS5** relative to **IM2**) and is exergonic by 43.9 kcal mol^{-1}.

3.2 Mechanism for biaryl formation

The mechanisms discussed above elucidate the generation of the borylated product. Interestingly, the over cross-coupling of **Pr1** leads to biaryl formation. The mechanism of the subsequent biaryl formation was investigated. From CO-coordinated Ar[Ni](CO)Bpin intermediate **IM10**, transmetalation, decarbonylation, and reductive elimination to deliver the final product and regenerate the active catalyst. Fig. 6 shows the energetics of these four steps; optimized geometries of key stationary points are provided in Fig. 7. The transmetalation process can proceed in a concerted or stepwise fashion, based on our previous studies,[24] we first considered a concerted mechanism, as illustrated by the four-membered **TS7**, the transmetalation proceeds by cleaving the Ni–F and B–C(aryl) bonds concurrently, giving **IM11** and FB(pin). Alternatively, for a stepwise mechanism, the electronic deficient boron of the **Pr1** moiety extracts the F atom *via* **TS11** to break the Ni–F bond, resulting in **IM15**. The calculated relative free energy of **TS11** is 1.8 kcal mol^{-1} lower than that of **TS7**. However, we found that the calculated free energy barrier of the B–C(aryl) bond cleavage and the formation of Ni–C bond *via* **TS12** is 6.0 kcal mol^{-1} higher than **TS7**, which revealed that stepwise mechanism is unfavorable. In the stepwise pathway, the steric clash between the bulky Bpin group and the phosphine ligand causes a destabilization, leading to the high energy barrier observed in **TS12**. This steric hindrance is absent in the concerted mechanism, allowing for a smoother transition. Thus, the concomitant cleavages of the two bonds (*i.e.* Ni–F and B–C(aryl) bonds) could intrinsically be easier than the sequential cleavages of the two bonds. Although the stepwise transmetalation takes the advantage of the favorable coordination interaction between oxygen in **Pr1** and nickel, which is indicated by the short lengths of Ni–O coordination bonds (2.08 Å in **TS11**), however the formation of **IM15**), where the Ni–F bond is broken before the B–C bond is fully formed and often less stable and requires additional energy to proceed to the next step. Further, we compared the charge of Ni in **TS7** (−0.74) and **TS12** (−0.65), suggesting that **TS7** may correlate with greater stabilization of the transition state due to stronger coordination of the ligand at the metal center, contributing to a lower activation energy. In **TS12** the steric clash between the Bpin moiety and the phosphine ligand causes a relatively high energy barrier than **TS7**. Similar to the above mechanism, from **IM11** the carbonyl migratory insertion requires rotating the aryl group *trans* to the carbonyl group, a very facial rotation along the Ni–C(aryl) bond of **IM11** preferentially takes place to form **IM12** *via* **TS8** which crosses a barrier of 14.9 kcal mol^{-1} relative to **IM11**. Then, a carbonyl migratory insertion proceeds *via* **TS9**, generating more stable the Ar[Ni](CO)Ar′ intermediate **IM13**. In **TS9** the distance of the breaking C–C bond (1.74 Å) and forming C–C bond (2.09 Å) confirm the formation of CO-coordinated intermediate **IM13** geometrically. Finally, **IM13** undergoes reductive elimination *via* **TS10**, affording the coupling product **Pr2** and regenerating the catalyst. Overall, based on the calculated free energy changes of the whole catalytic cycle, the resting

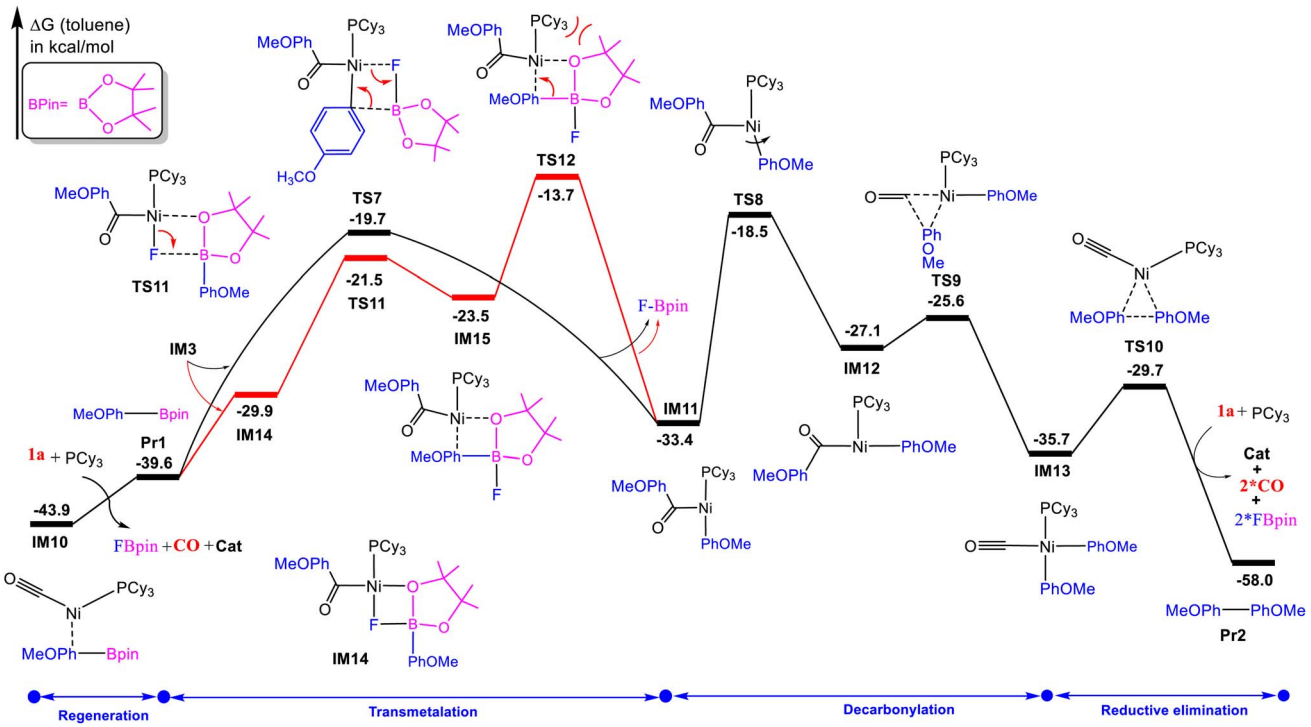

Fig. 6 Free-energy profiles for biaryl formation **Pr2**.

state of the cycle is the CO-coordinated Ar[Ni](CO)Bpin intermediate **IM10**, and the carbonyl migratory insertion has a rate-determining step (RDS) with a barrier of 25.4 kcal mol^{-1} (**TS8** relative to **IM10**) and is exergonic by 58.0 kcal mol^{-1}. Therefore, these results showed that the formation of biaryl product is thermodynamically more favorable than the organoboron product **Pr1**.

3.3 Origins for different chemoselectivity of part 1(b)

The mechanisms discussed above elucidate the base-free nickel catalyzed Suzuki–Miyaura cross-coupling of acid fluoride and diboron reagent to afford organoboron and biaryl. Analyzing the mechanisms in Fig. 3 and 4, we can find out that, the reaction undergoes sequential oxidative addition, transmetalation, decarbonylation, and reductive elimination. Comparing Fig. 4 and 6, the pathway leading to **Pr1** is somewhat similar to **Pr2**, although the decarbonylation and reductive elimination steps are somewhat different. In Fig. 4 the RDS is the rotation of Ni–B bond *via* **TS5**. Similarly, the RDS in Fig. 6 is the rotation of the Ni–C(aryl) bond of **IM11** *via* **TS8**. Fig. 4 and 6 provide valuable insights into the energetic results that help us understand the origin of chemoselectivity towards aryl boronate esters over biaryl compounds. The RDS barrier (**TS5**) to give aryl boronate ester (**Pr1**) is 2.0 kcal mol^{-1} lower than that (**TS8**) to give biaryl product (**Pr2**). We analyzed and compared the relative activation barriers ($\Delta G^{\ddagger}$) associated with the key steps in the reaction pathways of **TS5** and **TS8**. The activation barrier ($\Delta G^{\ddagger}$) for TS8 (~25 kcal mol^{-1}) relative to **IM10** is higher than that of **TS5** (~23 kcal mol^{-1}) relative to **IM2** (see Fig. 4 and 6), indicating that the PhOMe-containing intermediate overcomes a larger distortion energy to reach the transition state. To further investigate steric contributions, we performed a distortion interaction analysis on transition states (Fig. S4†). The bond angle at the nickel center is compressed for **TS8** (123°) compared to **TS5** (127°), and the dihedral angle between one of the PCy ligands, nickel, and the PhOMe moiety varies significantly from planar at 138° to 169° when considering the PCy ligand, nickel, and the BPin moiety. This variation indicates an increase in torsional strain. We also performed NBO (natural bond orbital) analysis to gain insight into the electronic environment of the nickel center. The NBO analysis shows the Ni in the **TS5** intermediate is slightly negative (−0.104), while in **TS8**, it is more positive (+0.18). This suggests greater electron donation from BPin due to its stronger σ-donor character. These findings reveal that **TS8** induces greater steric hindrance, resulting in a more distorted geometry and a less energetically favorable transition state compared to the BPin-containing system.Thus, part b of Fig. 1 reactions kinetically prefers to produce aryl boronate ester (**Pr1**), agreed with the experimental result.[23] Note that **Pr1** is thermodynamically less favorable than **Pr2**, thus the selectivity of aryl boronate ester of the reaction is exclusively controlled by kinetics. The chemoselective preference for the borylation product using the $B_2(Pin)_2$ substituent was attributed to the following factors: the electron-deficient boron creates an extra stabilization energy and lowers the free energy in **TS5**. In contrast, using **Pr1** as a substituent, the electronic and steric effect of PhOMe moiety in **TS8** destabilizes the biaryl formation kinetically. Overall, the chemoselectivity originates from the electronic and steric effects of BPin and PhOMe in **TS5** and **TS8**.

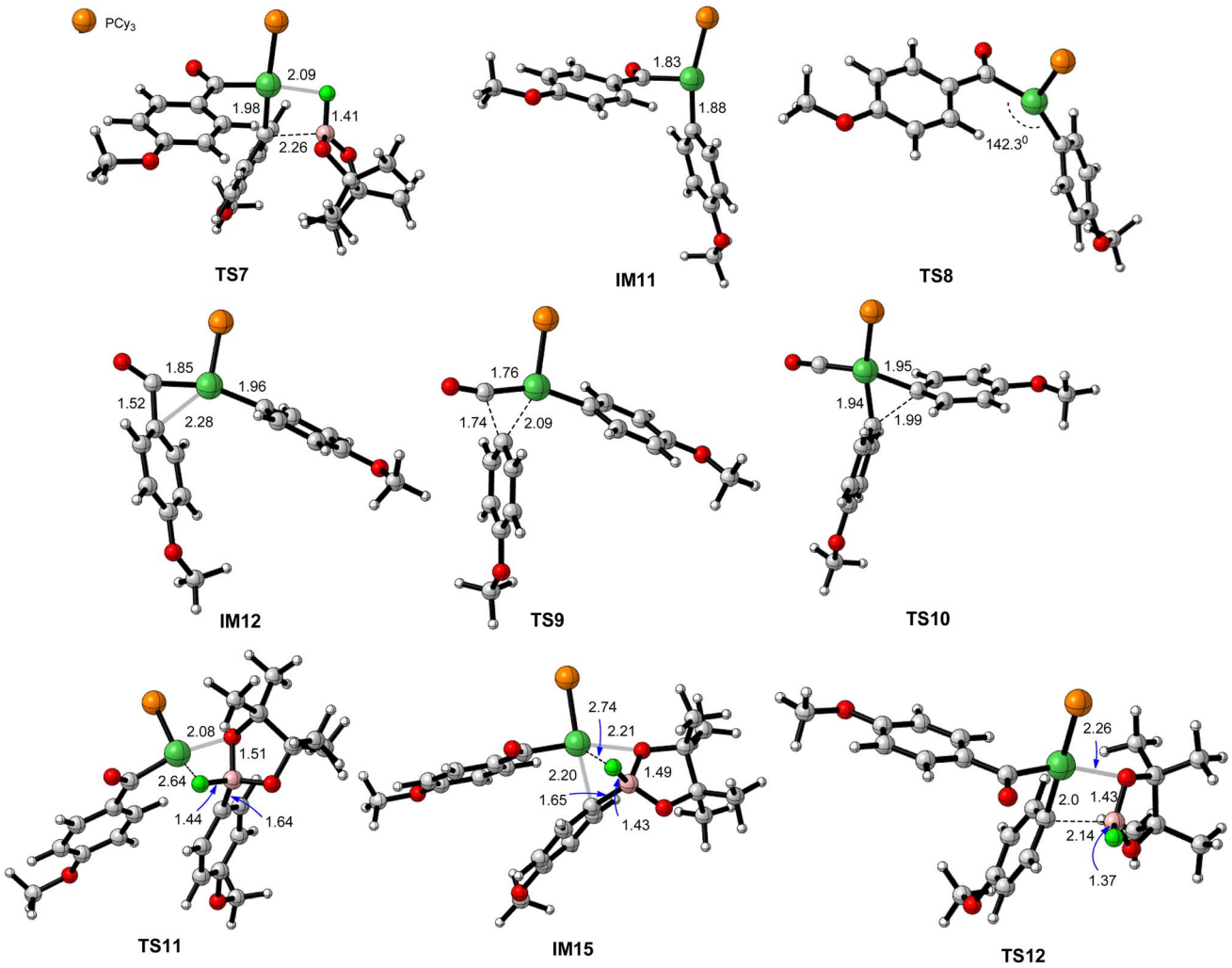

Fig. 7 Optimized structures of the key stationary points are displayed in Fig. 6.

4. Conclusion

In this study, we performed a DFT mechanistic study of a base-free nickel-catalyzed decarbonylative borylation of acid fluorides giving aryl boronate ester or biaryl selectively. The catalysis proceeds in four stages: (1) the oxidative addition of the acid fluoride substrate to $Ni^{(0)}$ center (2) transmetalation with diboron reagent. (3) Carbonyl deinsertion *via* reverse carbonyl migratory insertion. (4) Reductive elimination to afford the product and regenerate the active catalyst. In our computed mechanism, the transmetalation prefers a concerted mechanism and takes place first before carbonyl deinsertion which is different from the experimentally proposed mechanism. Importantly, the competitive rotation of Ni–B bond *via* **TS5** and Ni–C(aryl) bond of **IM1** *via* **TS8**, determines the chemoselectivity of the catalytic cycle and carbonyl migratory insertion is the rate-determining step of the coupling. The strong fluorophilicity of diboron assists the base free transmetalation. This study provides valuable insights that could contribute to the development of cost-effective catalysts for Suzuki–Miyaura cross-coupling reactions.

Data availability

The data supporting this article including *xyz* coordinates have been included as part of the ESI.†

Conflicts of interest

There are no conflicts to declare.

References

1 N. Miyaura and A. Suzuki, *Chem. Rev.*, 1995, **95**, 2457–2483.
2 C. C. C. Johansson Seechurn, M. O. Kitching, T. J. Colacot and V. Snieckus, *Angew. Chem., Int. Ed.*, 2012, **51**, 5062–5085.
3 C. M. So and F. Y. Kwong, *Chem. Soc. Rev.*, 2011, **40**, 4963–4972.
4 R. Takise, K. Muto and J. Yamaguchi, *Chem. Soc. Rev.*, 2017, **46**, 5864–5888.
5 M. Mondal, T. Begum and U. Bora, *Org. Chem. Front.*, 2017, **4**, 1430–1434.
6 A. Suzuki, *Angew. Chem., Int. Ed.*, 2011, **50**, 6722–6737.

7 D. G. Brown and J. Boström, *J. Med. Chem.*, 2016, **59**, 4443–4458.
8 R. Renzo, B. Fabio, L. Marco, M. Chiara, M. Giulia and A. P. Luca, *Curr. Org. Chem.*, 2015, **19**, 1302–1409.
9 A. Taheri Kal Koshvandi, M. M. Heravi and T. Momeni, *Appl. Organomet. Chem.*, 2018, **32**, e4210.
10 A. J. J. Lennox and G. C. Lloyd-Jones, *Angew. Chem., Int. Ed.*, 2013, **52**, 7362–7370.
11 P. A. Cox, M. Reid, A. G. Leach, A. D. Campbell, E. J. King and G. C. Lloyd-Jones, *J. Am. Chem. Soc.*, 2017, **139**, 13156–13165.
12 F.-S. Han, *Chem. Soc. Rev.*, 2013, **42**, 5270–5298.
13 J. Yamaguchi, K. Muto and K. Itami, *Eur. J. Org Chem.*, 2013, **2013**, 19–30.
14 S. Z. Tasker, E. A. Standley and T. F. Jamison, *Nature*, 2014, **509**, 299–309.
15 V. P. Ananikov, *ACS Catal.*, 2015, **5**, 1964–1971.
16 Z. Li and L. Liu, *Chin. J. Catal.*, 2015, **36**, 3–14.
17 L. Guo and M. Rueping, *Acc. Chem. Res.*, 2018, **51**, 1185–1195.
18 M. Ohashi, H. Saijo, M. Shibata and S. Ogoshi, *Eur. J. Org Chem.*, 2013, **2013**, 443–447.
19 N. Blanchard and V. Bizet, *Angew. Chem., Int. Ed.*, 2019, **58**, 6814–6817.
20 Y. Ogiwara, D. Sakino, Y. Sakurai and N. Sakai, *Eur. J. Org Chem.*, 2017, **2017**, 4324–4327.
21 Y.-Y. Sun, J. Yi, X. Lu, Z.-Q. Zhang, B. Xiao and Y. Fu, *Chem. Commun.*, 2014, **50**, 11060–11062.
22 C. A. Malapit, J. R. Bour, C. E. Brigham and M. S. Sanford, *Nature*, 2018, **563**, 100–104.
23 C. A. Malapit, J. R. Bour, S. R. Laursen and M. S. Sanford, *J. Am. Chem. Soc.*, 2019, **141**, 17322–17330.
24 C. Zhang, R. Zhao, W. M. Dagnaw, Z. Liu, Y. Lu and Z.-X. Wang, *Theor. Chim. Acta*, 2019, **84**, 13983–13991.
25 M. J. Frisch, G. W. Trucks, H. B. Schlegel, G. E. Scuseria, M. A. Robb, J. R. Cheeseman, G. Scalmani, V. Barone, B. Mennucci, G. A. Petersson, H. Nakatsuji, M. Caricato, X. Li, H. P. Hratchian, A. F. Izmaylov, J. Bloino, G. Zheng, J. L. Sonnenberg, M. Hada, M. Ehara, K. Toyota, R. Fukuda, J. Hasegawa, M. Ishida, T. Nakajima, Y. Honda, O. Kitao, H. Nakai, T. Vreven, J. A. Montgomery Jr, J. E. Peralta, F. Ogliaro, M. Bearpark, J. J. Heyd, E. Brothers, K. N. Kudin, V. N. Staroverov, R. Kobayashi, J. Normand, K. Raghavachari, A. Rendell, J. C. Burant, S. S. Iyengar, J. Tomasi, M. Cossi, N. Rega, J. M. Millam, M. Klene, J. E. Knox, J. B. Cross, V. Bakken, C. Adamo, J. Jaramillo, R. Gomperts, R. E. Stratmann, O. Yazyev, A. J. Austin, R. Cammi, C. Pomelli, J. W. Ochterski, R. L. Martin, K. Morokuma, V. G. Zakrzewski, G. A. Voth, P. Salvador, J. J. Dannenberg, S. Dapprich, A. D. Daniels, Ö. Farkas, J. B. Foresman, J. V. Ortiz, J. Cioslowski and D. J. Fox, *Gaussian 09*, Gaussian, Inc., Wallingford, CT, 2009.
26 C. T. Lee, W. T. Yang and R. G. Parr, *Phys. Rev. B*, 1988, **37**, 785–789.
27 A. D. Becke, *J. Chem. Phys.*, 1993, **98**, 5648–5652.
28 Y. Zhao and D. G. Truhlar, *Acc. Chem. Res.*, 2008, **41**, 157–167.
29 P. C. Hariharan and J. A. Pople, *Theor. Chim. Acta*, 1973, **28**, 213–222.
30 W. J. Hehre, R. Ditchfield and J. A. Pople, *J. Chem. Phys.*, 1972, **56**, 2257–2261.
31 R. Ditchfield, W. J. Hehre and J. A. Pople, *J. Chem. Phys.*, 1971, **54**, 724–728.
32 L. E. Roy, P. J. Hay and R. L. Martin, *J. Chem. Theory Comput.*, 2008, **4**, 1029–1031.
33 D. Andrae, U. Häußermann, M. Dolg, H. Stoll and H. Preuß, *Theor. Chim. Acta*, 1990, **77**, 123–141.
34 Y. Zhao and D. G. Truhlar, *J. Chem. Theory Comput.*, 2009, **5**, 324–333.
35 A. D. Kulkarni and D. G. Truhlar, *J. Chem. Theory Comput.*, 2011, **7**, 2325–2332.
36 P. Śliwa and J. Handzlik, *Chem. Phys. Lett.*, 2010, **493**, 273–278.
37 A. V. Marenich, C. J. Cramer and D. G. Truhlar, *J. Phys. Chem. B*, 2009, **113**, 6378–6396.
38 U. Domańska, M. Laskowska and A. Pobudkowska, *J. Phys. Chem. B*, 2009, **113**, 6397–6404.
39 C. Y. Legault, *CYLView, Version 1.0 B*, Université de Sherbrooke, Sherbrooke, Quebec, Canada, 2009.